# APPLICATION OF CARRIER-ESPI FOR MEASUREMENT OF OUT-OF-PLANE DISPLACEMENTS IN UNSTITCHED AND STITCHED LAMINATES SUBJECTED TO COMPRESSION-AFTER-IMPACT

J.T. Ruan[1], D. Feng[2], F. Aymerich[2], J.W. Tong[1*], P.Priolo[2]

[1]*Department of Mechanics, University of Tianjin, China*
[2]*Department of Mechanical, Chemical and Materials Engineering, University of Cagliari, Italy*
* *tjw@tju.edu.cn*

**Keywords:** Compression after impact; stitching; electronic speckle pattern interferometry; deformation.

## Abstract
*The carrier electronic speckle pattern interferometry (carrier-ESPI) optical method was used in this study to measure and compare out-of-plane displacements under compression of unstitched and stitched composite plates containing delaminations induced by low velocity impact. $[0_3/90_3]_S$ graphite/epoxy laminates were impacted using a drop-weight testing machine and then subjected to compression after impact tests. Carrier-ESPI results show that the buckling behaviour of both unstitched and stitched laminates is characterized by a mixed (global and local) mode shape at high compressive loads. Optical measurements also highlight the restraining effect on local buckling displacements exerted by stitches bridging the delamination crack.*

## 1 Introduction
Composite materials are widely used in many engineering applications because of their high specific tensile/compressive strength and of their excellent corrosion resistance properties. Laminated composites are however very sensitive to impact loads along the thickness direction, which may induce a combination of damage modes (matrix cracking, delamination, fibre fracture [1]) likely to result in serious degradation of the load-carrying capability of the material. Delaminations are especially dangerous for a composite structure, because they increase the sensitivity to buckling phenomena and may thus lead to significant reduction in compressive strength. In this respect, it has been shown that the delamination resistance and the compression after impact (CAI) strength of laminated structures can be improved considerably by the insertion of through-thickness reinforcement by stitching or z-pinning [2,3].
Many numerical and experimental studies have been conducted to characterize the buckling behaviour and the compression response of delaminated composite plates. The effects of the presence of a delamination on the buckling load and on associated mode shapes of composite laminates under compression were for example studied in [4-6] by means of analytical models or by 2D and 3D finite element analyses. Likewise, the tolerance to impact-induced delaminations was characterized experimentally in numerous investigations (see for example [7-9]) with the use of various measuring techniques and different anti-buckling support fixtures. Analogous experimental approaches were adopted to characterize the influence of

through-thickness reinforcement on the compression after impact (CAI) strength of composite laminates [10-12].

With reference to experimental analyses, non-contact optical methods, which may provide high-precision full-field information, have been often applied for measurement of the displacement field in composite materials. Cairns et al. [13] characterized the out-of-plane displacements of composite laminates with artificially manufactured delaminations under in-plane compressive loads via shadow moiré. Golda et al. [14] developed an adaptive electronic speckle pattern interferometry (ESPI) system to measure the out-of-plane deformation of laminates subjected to quasi-static loads. Farge et al. [15] used ESPI and phase-shifting to measure the full-field displacement at the edge of a laminated specimen with multiple transverse cracks.

The objective of this study is to experimentally investigate the deformation behaviour under compressive loading of unstitched and stitched composite laminates with impact damage using a carrier electronic speckle pattern interferometry (carrier-ESPI) optical technique. Because of the introduction of carrier fringes, the carrier-ESPI method can directly obtain the phase field without any phase shifter. The specimens were first impacted with a drop weight impact testing machine and then subjected to CAI tests using an anti-buckling support fixture. The out-of-plane displacements of impacted specimens were finally observed and measured by carrier-ESPI, with the aim of characterizing the buckling behaviour of impacted laminates and of gaining insight into the role of through-thickness stitches on the compressive response of the damaged material.

## 2 Experimental details

### *2.1 Materials and specimen*

A cross-ply $[0_3/90_3]$s graphite/epoxy laminate was examined in this study. Laminated panels were first fabricated from Seal Texipreg HS160/REM graphite/epoxy prepreg tapes and then cured in an autoclave at a maximum temperature of 160 °C. The average thickness of the cured panels was 2.0 mm and the nominal fibre fraction of prepreg layers was 61.5% in weight. Some of the laminated panels were stitched before curing with Kevlar-29 untwisted rovings (220 dtex) using an industrial sewing machine. A modified lock stitch was employed here to minimize the effect of damage to the prepreg fibres. Samples were stitched perpendicularly to the 0° direction of the laminate, with a 5mm space between adjacent stitching lines and between consecutive stitches along stitching lines [12]. All laminates used in the experiments were finally cut from the composite plates into rectangular specimens 65 mm × 87.5 mm in size. The geometry and the stitching pattern of composite samples are shown in Fig. 1.

An instrumented drop weight testing machine with a 2.28 kg impactor provided with a hemispherical steel tip of 12.5 mm diameter was used for the low velocity impact tests. The contact force between impactor and specimen was measured by means of a semiconductor strain-gauge bridge bonded to the impactor rod.

After impact, internal damage was non-destructively examined by means of penetrant enhanced X-ray radiography. As visible in the X-rays of Fig. 2, the typical damage induced by impact in this class of laminates [12] consists of matrix cracking in 0° and 90° layers and of an extensive delaminated area at the 90/0 interface close to the backface of the sample.

### *2.2 Antibuckling fixture*

The fixture designed and adopted for CAI tests, shown in Fig. 3, uses two anti-buckling steel plates with a square opening of 29.4 mm × 67 mm to reduce global buckling phenomena. The two steel plates are clamped in a slot at the base of the fixture, and supported at both sides by two side plates with knife edges. The gap between the knife edges can be adjusted to hold specimens with different thicknesses. The impacted laminates were mounted into the anti-buckling device with the 0° fibre direction parallel to the loading (y) direction.

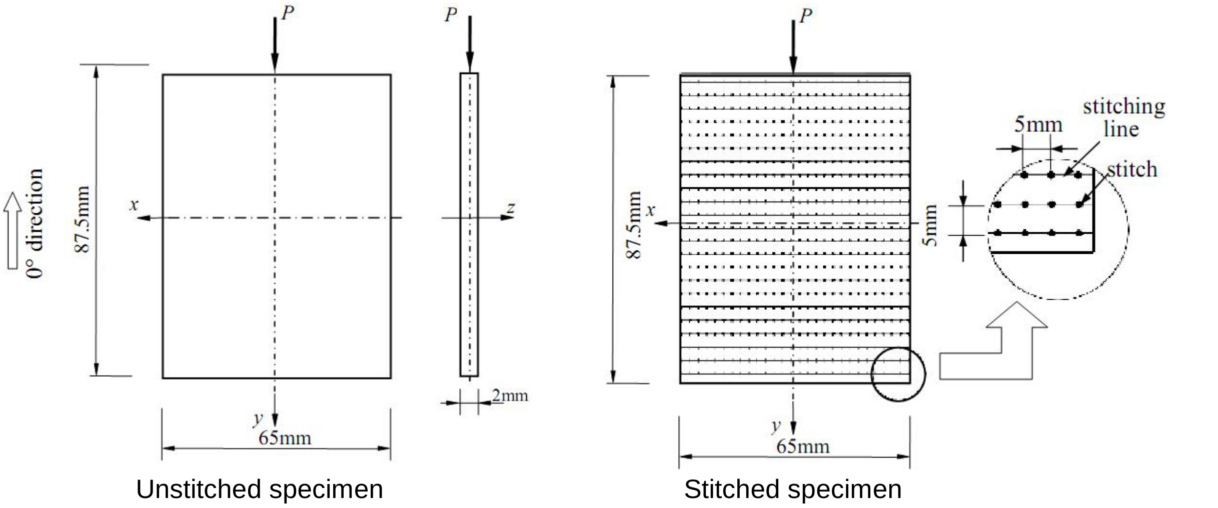


**Figure 1.** Geometry and stitching pattern of composite specimens

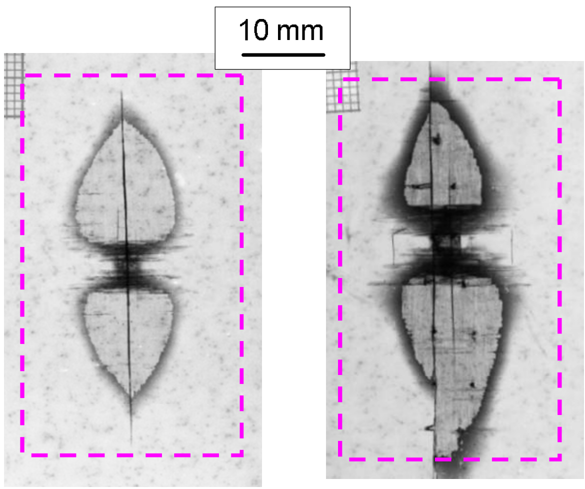


**Figure 2.** X-radiographs of damage in an unstitched (left; impact energy = 6.7 J) and stitched (right; impact energy = 10 J) laminate. The dashed rectangle indicates the measurement area

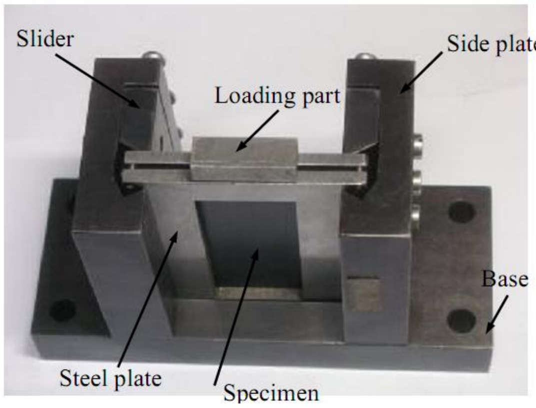


**Figure 3.** Antibuckling fixture

## *2.3 Carrier ESPI technique*

A measurement area 28 × 44 mm$^2$ in size and centred around the impact point (see Fig. 2) was chosen to measure the displacements of the damaged portion of the specimen with the carrier-ESPI technique. The schematic diagram of the experimental setup is shown in Fig. 4. The setup uses a conventional electronic speckle pattern interferometry optical arrangement with sensitivity to the out-of-plane displacement component *w* of the specimen.

During the experiments, a beam of a 30 mW He-Ne laser with a wavelength of 0.6328 μm was sent through an expander and a spatial filter and divided into two beams by a 50/50 beam splitter. The two expanded beams were used to illuminate the specimen under study and the reference object, respectively. The beams from the specimen and the reference object met again at the beam splitter to interfere with each other. This interference reached the CCD camera (with the axis aligned along the z-axis direction), which was connected to a personal computer with a digital image grabbing card in order to record the intensity distribution.

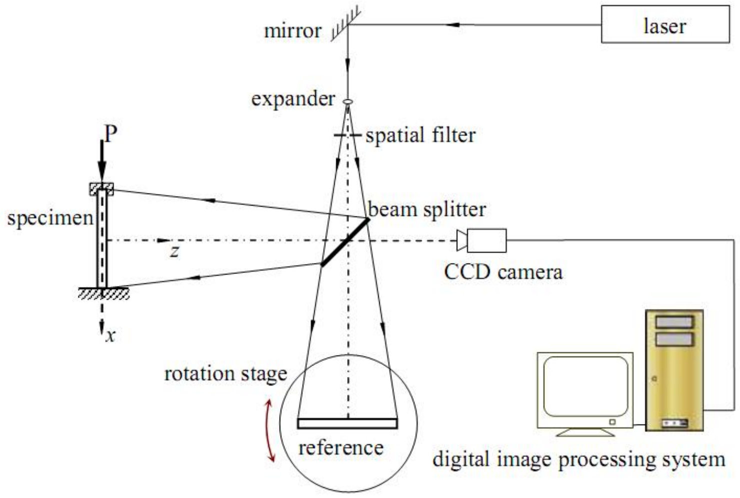


**Figure 4.** Schematic diagram of the experimental setup for carrier-ESPI

In order to generate the carrier fringes, the reference object was mounted on a precision rotation table in the x-z plane, and rotated around the y-axis by a very small angle. If the specimen was unloaded, the correlation fringe pattern showed a set of equispaced parallel vertical fringes, whose spatial frequency $f_0$ was proportional to the magnitude of rotation angle. By contrast, the carrier fringes appeared to be curved when modulated by the deformation of sthe pecimen [16].

The experimental procedure of carrier-ESPI requires the acquisition of three speckle images, which correspond to different states of the specimen surface. The first specklegram $S_0$, which is recorded with the unloaded specimen, can be expressed mathematically as follows

$$I_0(x, y) = I_o(x, y) + I_r(x, y) + 2\sqrt{I_o(x, y)I_r(x, y)}\cos q(x, y) \tag{1}$$

where $I_0(x, y)$ is the intensity at a point $(x, y)$ of the specklegram. $Io(x, y)$ and $Ir(x, y)$ are the intensities at the point $(x, y)$ of the object and reference beam, respectively. $q(x, y)$ is the random phase difference of the recorded specklegram.

The second specklegram $S_1$ which is recorded after the reference object is rotated by a small angle, can be written as the following expression

$$I_1(x, y) = I_o(x, y) + I_r(x, y) + 2\sqrt{I_o(x, y)I_r(x, y)}\cos[q(x, y) + 2p\ f_0 x] \tag{2}$$

where $f_0$ is the spatial carrier frequency along the x direction introduced by rotating the reference object, and $2p\, f_0\, x$ is the carrier phase field.

The third speckle gram $S_2$ which is recorded after the specimen is loaded, can be expressed as

$$I_2(x, y) = I_o(x, y) + I_r(x, y) + 2\sqrt{I_o(x, y)I_r(x, y)}\cos[q(x, y) + 2p\ f_0 x + \Delta f(x, y)] \tag{3}$$

where $Df(x, y)$ is the phase term of interest caused by the deformation of the specimen.

The pure carrier fringe pattern is obtained by subtracting the specklegram $I_0(x, y)$ from $I_1(x, y)$ and taking the squared value of the intensity difference.

$$I_{10}(x,y) = \left[I_1(x,y) - I_0(x,y)\right]^2 = 8 I_o(x,y) I_r(x,y) \sin^2\left[q(x,y) + p\ f_0 x\right]\left[1 - \cos(2p\ f_0 x)\right] \quad (4)$$

Neglecting the speckle noise term in the correlation fringe pattern, the upper expression can be written approximately as

$$I_{10}(x,y) = a(x,y) + b(x,y)\cos\left(2p\ f_0 x\right) \quad (5)$$

where *a(x, y)* represents the background intensity, *b(x, y)* is the visibility of the fringes. Similarly, subtraction of the speckle image $I_0(x, y)$ from $I_2(x, y)$ can yield a deformation carrier fringe pattern, which can be written as

$$I_{20}(x,y) = a(x,y) + b(x,y)\cos\left[2p\ f_0 x + \Delta f(x,y)\right] \quad (6)$$

The phase field is retrieved from the pure and deformation carrier fringe patterns by the Fourier transform method (FTM), a technique originally demonstrated by Takeda et al. [17]. The Fourier transform with respect to x-axes of Eq. (5) yields

$$H(f_x, y) = A(f_x, y) + C(f_x - f_0, y) + C^*(f_x + f_0, y) \quad (7)$$

Where, ∗ denotes the complex conjugate; $A(f_x, y)$ is the zero frequency spectrum term; $C(f_x\text{-}f_0, y)$ and $C^*(f_x+f_0, y)$ denote frequency spectrum terms with a deviation of $\pm f_0$ from the carrier frequency. By properly using a filtering window in the Fourier spectrum, we can isolate one of the two sidebands, i.e. $C(f_x\text{-}f_0, y)$, and then the inverse Fourier transform is applied on this term to obtain

$$c_1(x,y) = \frac{1}{2} b(x,y)\exp(j2p\ f_0 x) \quad (8)$$

Taking out the real and imaginary parts of above expression, the phase distribution of the pure carrier fringe pattern can be calculated by

$$2p\ f_0 x = \tan^{-1}\frac{\mathrm{Im}[c_1(x,y)]}{\mathrm{Re}[c_1(x,y)]} \quad (9)$$

Where Re[ ] and Im[ ] denote the real and imaginary parts of $c_1(x,y)$ from Eq. (8), respectively.
Similarly, applying FTM on Eq. (6), the phase distribution of the deformation carrier fringe pattern can be obtained

$$2p\ f_0 x + \Delta f(x,y) = \tan^{-1}\frac{\mathrm{Im}[c_2(x,y)]}{\mathrm{Re}[c_2(x,y)]} \quad (10)$$

where

$$c_2(x,y) = \frac{1}{2} b(x,y)\exp[j\Delta f(x,y)]\exp(j2p\ f_0 x) = \frac{1}{2} b(x,y)\exp[j(2p\ f_0 x + \Delta f(x,y))] \quad (11)$$

The Eq. (9) subtracted from Eq. (10) gives the deformed phase field, which is a wrapped phase field. The unwrapped phase field can be finally determined with the use of a phase unwrapping algorithm [18]. According to the optical arrangement, as shown in Fig. 4, the out-of-plane displacement of specimen is calculated as

$$w = \frac{l}{4p} \Delta f(x, y) \tag{12}$$

where $l$ is the wavelength of the laser beam.

## 3 Experimental results

Figs. 5 reports selected experimental results as obtained by carrier-ESPI from CAI tests on impact-damaged unstitched and stitched samples. The left column of Fig. 5 shows out-of-plane displacement maps obtained on an unstitched composite sample impacted with an energy of 6.7 J (the X-radiograph of the internal damage is shown in Fig. 2) and subjected to increasing compressive loads. We may observe that the deformation behaviour is characterized by a global buckling mode at low compressive loads. As the applied load increases, local buckling of the sublaminates generated by impact delaminations also occur around the impact locations, thus giving rise to a global-local buckling mode.

Out-of-plane displacements of a stitched sample damaged by a 10 J energy impact are illustrated in the right column of Fig. 5. We may see that in impacted stitched laminates the initial deformation mode is again associated to global buckling of the sample, followed –at higher compressive loads- by local buckling of the delaminated lobes, with a mixed-mode deformation shape. The displacement maps of stitched specimens also clearly show the restraining effect played by stitching on out-of-plane displacements generated to local buckling instabilities, as a direct result of the bridging action exerted by intact stitches on the sublaminates at the delaminated areas. The beneficial action of stitching reinforcement on the compressive response of the laminates is also indicated by the maximum values of out-of plane displacements, which are close to those measured for the unstitched specimens, in spite of the significantly larger delaminated area of the stitched sample.

## 4 Conclusions

The carrier-ESPI technique has been applied for full-field measurement of out-of-plane displacements in unstitched and stitched graphite/epoxy laminates subjected to compression after impact. Based on the experimental results, the following main conclusions can be drawn:

- In both unstitched and stitched laminates the deformation behaviour appears characterized by a global buckling mode at low compressive load, followed by local buckling of sublaminates at higher loads.
- The displacement maps obtained by carrier-ESPI clearly demonstrate the restraining effect exerted by stitches on displacements associated to local buckling instabilities.
- The carrier-ESPI technique has been demonstrated as a highly sensitive experimental technique for the analysis of the buckling behaviour of impact-damaged laminates, and as an effective tool for the assessment of the effect of stitching on the damage tolerance of impacted laminates.

**Acknowledgements**

The authors are grateful to the European Union (FP7-ITN-Marie Curie project SYSWIND - Grant No. FP7-PEOPLE-ITN 238325), to the National Natural Science Foundation of China (Grant Nos 11072174, 10972155 and 10572103) and to the University of Cagliari (Visiting Professors program funded by the Regional Government of Sardinia) for financial support.

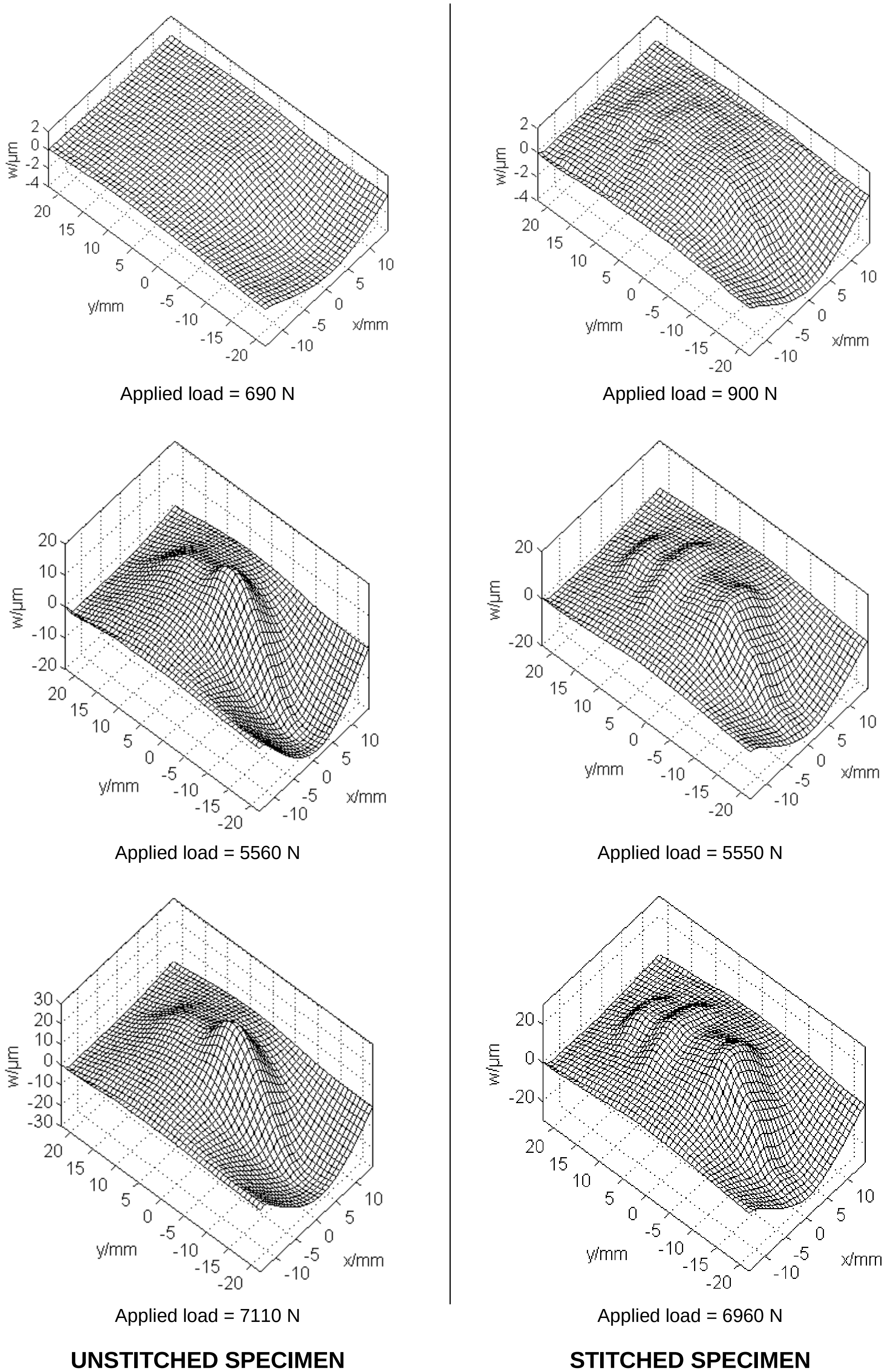


**Figure 5.** Out-of-plane displacement field at increasing compressive loads

## References

[1] Finn S.R., He Y.F. Springer G.S. Delaminations in composite plates under transverse impact loads–Experimental results. *Composite Structures*, **23**, pp. 191-204 (1993).
[2] Mouritz A.P., Leong K.H., Herszberg I. A review of the effect of stitching on the inplane mechanical properties of fibre–reinforced polymer composites. *Composites Part A*, **28**, pp. 979-991 (1997).
[3] Dransfield K., Baillie C., Mai Y.W. Improving the delamination resistance of CFRP by stitching – a review, *Composites Science and Technology*, **50**, pp. 305-317 (1994).
[4] Kim H., Kedward K.T.,A method for modeling the local and global buckling of delaminated composite plates, *Composite Structures*, **44**, pp. 43-53 (1999).
[5] Gaudenzi P. On delamination buckling of composite laminates under compressive loading, *Composite Structures*, **39**, pp. 21-30 (1997).
[6] Tafreshi A., Oswald T. Global buckling behaviour and local damage propagation in composite plates with embedded delaminations, *International Journal of Pressure Vessels and Piping*, **80**, pp. 9-20 (2003).
[7] Sanchez S.S., Barbero E., Zaera R., Navarro C. Compression after impact of thin composite laminates, *Composites Science and Technology*, **65**, pp. 1911-1919 (2005).
[8] Zhang X., Davies G.A.O., Hitchings D. Impact damage with compressive preload and post-impact compression of carbon composite plates, *International Journal of Impact Engineering* , **22**, pp. 485-509 (1999).
[9] Heimbs S., Heller S., Middendorf P., Hähnel F., Weiße J. Low velocity impact on CFRP plates with compressive preload: Test and modelling, *International Journal of Impact Engineering* , **36(10-11),** pp. 1182–1193 (2009).
[10] Cheng X.Q., Al-Mansour A.M., Li Z.N., Kou C.H. Compression strength of stitched laminates after low-velocity impact. *Journal of Reinforced Plastics and Composites*, **24(9)**, pp. 935–47 (2005).
[11] Tan K.T., Watanabe N., Iwahori Y., Ishikawa T. Effect of stitch density and stitch thread thickness on compression after impact strength and response of stitched composites, *Composites Science and Technology*, **72**, pp. 587–598 (2012).
[12] Aymerich F., Priolo P. Characterization of fracture modes in stitched and unstitched cross-ply laminates subjected to low-velocity impact and compression after impact loading, *International Journal of Impact Engineering*, **35**, pp. 591-608 (2008).
[13] Cairns D.S., Minguet P.J., Abdallaha M.G. Theoretical and experimental response of composite laminates with delaminations loaded in compression, *Composite Structures*, **24**, pp. 431-437 (1994).
[14] Golda D., Kedlaya D., Pelegri A.A. Deflection measurements of laminated thin plates using electronic speckle pattern interferometry, *Journal of Composites Technology and Research*, **24(4),** pp. 215-223 (2002).
[15] Farge L., Ayadi Z. and Varna J. Optically measured full-field displacements on the edge of a cracked composite laminate, *Composites Part A: Applied Science and Manufacturing*, **39(8)**, pp. 1245-1252 (2008).
[16] Sun P. The separation of out-of-plane displacement from in-plane components by fringe carrier method based on large image-shearing ESPI, *Optics Communications*, **275**, pp. 305-310 (2007).
[17] Takeda M., Ina H., Koboyashi S. Fourier-transform method of fringe-pattern analysis for computer based topography and interferometry. *Journal of the Optical Society of America A*, **72**, pp. 156-160 (1982).
[18] Judge T.R., Bryanston-Cross P.J. A review of phase unwrapping techniques in fringe analysis, *Optics and Lasers in Engineering*, **21**, pp. 199-239 (1994).